Wind and Structures, *Vol. 30, No. 4 (2020) 325-338*
DOI: https://doi.org/10.12989/was.2020.30.4.325

Optimization of the anti-snow performance of a high-speed train based on passive flow control

Guangjun Gao[1,2,3a], Zhen Tian[1,2,3b], Jiabin Wang[*1,2,3], Yan Zhang[1,2,3c], Xinchao Su[1,2,3d] and Jie Zhang[1,2,3e]

[1]*Key Laboratory of Traffic Safety on Track of Ministry of Education, School of Traffic & Transportation Engineering, Central South University, Changsha 410075, China*
[2]*Z2Joint International Research Laboratory of Key Technology for Rail Traffic Safety, Central South University, Changsha 410075, China*
[3]*National & Local Joint Engineering Research Center of Safety Technology for Rail Vehicle, Changsha 410075, China*

(Received August 2, 2019, Revised October 14, 2019, Accepted October 18, 2019)

Abstract. In this paper, the improvement of the anti-snow performance of a high-speed train (HST) is studied using the unsteady Reynolds-Averaged Navier-Stokes simulations (URANS) coupled with the Discrete Phase Model (DPM). The influences of the proposed flow control scheme on the velocity distribution of the airflow and snow particles, snow concentration level and accumulated mass in the bogie cavities are analyzed. The results show that the front anti-snow structures can effectively deflect downward the airflow and snow particles at the entrance of the cavities and alleviate the strong impact on the bogie bottom, thereby decrease the local accumulated snow. The rotational rear plates with the deflecting angle of 45° are found to present well deflecting effect on the particles' trajectories and force more snow to flow out of the cavities, and thus significantly reduce the accretion distribution on the bogie top. Furthermore, running speeds of HST are shown to have a great effect on the snow-resistance capability of the flow control scheme. The proposed flow control scheme achieves more snow reduction for HST at higher train's running speed in the cold regions.

Keywords: bogie cavity; High-Speed Train (HST); numerical simulation; passive flow control

1. Introduction

Nowadays, HST has become one of the most popular means of transportation thanks to its high capacity and efficiency. For some countries having advanced HST techniques, many high-speed railways have been built in the snowy areas. Such as the Harbin-Mudanjiang High-speed Railway and Qinhuangdao-Shenyang High-speed Railway in China, Kyushu and Akita Shinkansen in Japan, Helsinki-Tampere High-speed Railway in Finland and Frankfurt-Cologne High-speed Railway in Germany etc. When HSTs run on these railways, the high-speed slipstream beneath the HSTs will roll up the snow particles from the ballast, leading to massive snow accretion in the bogie cavities of HSTs (Casa *et al*. 2014, Wang *et al*. 2017), as shown in Fig. 1. The snow packing on the bogies, such as the motors, gear covers, elastic suspensions and brake devices, has been found to significantly deteriorate the comfort of passengers and even threaten the running safety of HSTs (Xie *et al*. 2017, Kosinski and Hoffmann 2007, Casa *et al*. 2014, Giappino *et al*. 2016).

Aiming at the solutions for the snow issue of HST, the researchers in the related field have conducted a great number of studies and proposed several contra-measures. The first contra-measure is to decrease the snow accumulation on the subgrade. Some examples are the high-efficiency snow-removal viaducts (Fujii *et al.* 2002) and spraying devices (Thomas 2009) in Japan, snow fences in Norway (Bettez 2011) and the anti-snow brushers in Sweden (Bettez 2011). However, these snow-resistance technologies can not totally remove the accumulated snow from the subgrade, and the snow issue still occurs in the bogie cavities after long-time operation of HSTs. The second measure is to develop heating technologies to melt the snow packing on bogies. Some solutions are the hot propylene glycol (Bettez 2011), hot water (Bettez 2011), propylene aqueous solution (Paulukuhn 2012) and the hot air (Wang *et al.* 2018a). The contra-measures belongs to the second group can only melt the snow accumulation for the HSTs stopping in the vehicle depots, while the HSTs running on the railways in the cold regions are still threatened by this snow issue.

Based on the discussions above, the snow issue needs other solutions to ensure the running safety of HSTs. At present, investigating attentions are concentrated on the passive flow control schemes to improve the anti-snow

*Corresponding author, Ph. D
E-mail: wangjiabin@csu.edu.cn
[a]Professor
E-mail: gjgao@csu.edu.cn
[b]Ms. C
E-mail: 184212086@csu.edu.cn
[c]Ph. D
E-mail: 1062426943@qq.com
[d]Ph. D
E-mail: suxinchao@csu.edu.cn
[e]Professor
E-mail: jie_csu@csu.edu.cn

ISSN: 1226-6116 (Print), 1598-6225 (Online)

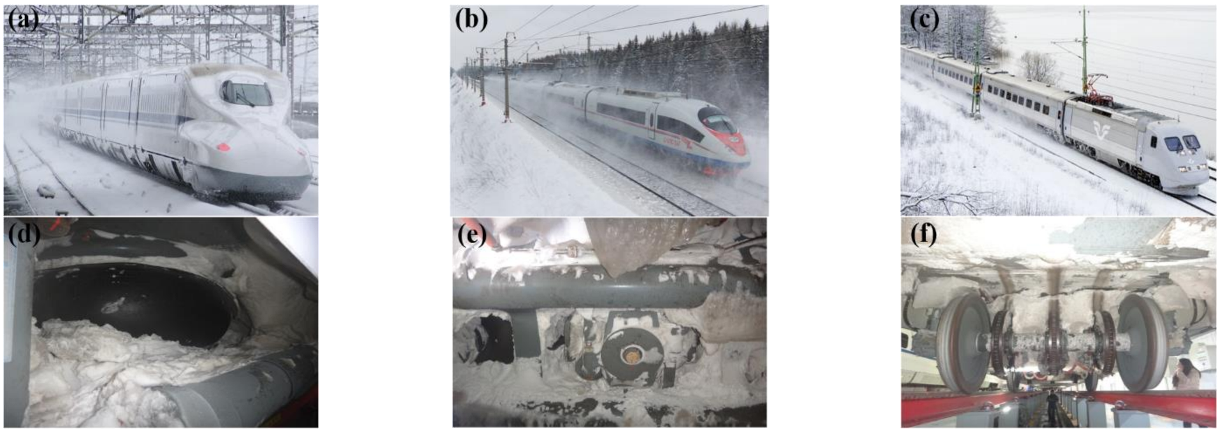

Fig. 1 The snow issue in the bogie cavities of HSTs

performance of the HSTs. Wang *et al.* (2018c) designed two types of deflectors to optimize the trajectories of the wind-snow flow at the entrance of the cavities, and achieved about 38% snow reduction for a single bogie. Gao *et al.* (2018a) evaluated the effects of the shapes of equipment cabin covers on the snow-resistance ability of the HSTs, and significantly decreased the snow accretion inside the cavities. Miao and He (2018) installed the triangular prism diversion slots at the upstream and downstream sides of the cavities, and reduced the airflow entering the cavities by 46.51%. Ding *et al.* (2016) proposed the rubber guiding plates for HSTs to incline downward the airflow near the cavity entrance and thereby optimize the particles' trajectories and relieve the snow issue for HSTs. Despite these optimizations, there is still much work to be done for the improvement of anti-snow performance of the HSTs.

The motivation of the present study is twofold. The guiding structures mentioned above primarily focus on the optimization of the trajectories of the snow at the entrance of the cavities, while less attention was paid on the outlet of the cavities. The deflectors installed downstream the bogies have a significant blocking effect on the snow particles at the outlet and thereby results in additional snow accretion. The first motivation is to propose a combined flow control scheme to optimize the trajectories of airflow and snow particles at both entrance and outlet of the cavities and achieve more snow reduction for HSTs. Furthermore, limited by the computational costs, Wang *et al.* (2018) and Gao *et al.* (2018a) used the coupled numerical method URANS and DPM to evaluate the anti-snow performance of the deflectors for a simplified vehicle with single bogie, while the effects of the streamlined shape and cowcatchers on the flow features of the airflow and snow particles were not considered. Moreover, previous studies conducted by Miao and He (2018) and Ding *et al.* (2016) have not considered the motion of the snow particles in the numerical simulation, and thereby fail to provide a quantitative analysis of the effects of the anti-snow structures on the snow reduction. Thus, the second motivation is to provide a supplement research to the snow issue of HST concerning how the combined flow control scheme affects the snow accretion of a three-car grouped HST.

The remainder of this paper is organized as follows: in Section 2, the HST model, domain, boundary conditions, meshes, the results of the grid independence and numerical methods are given together. In Section 3, the comparative analysis of the underbody air flow and snow motion between the original and optimized cases are conducted, and the capability of the anti-snow flow control scheme is also studied at higher running speeds. Finally, conclusions are drawn in Section 4.

2. Numerical set-up

2.1 HST model

A full-scale three-car grouped Chinese Standard HST is used in the present numerical simulations. The HST model consists of head car, middle car, tail car, two inter-carriage gaps and six bogies, as depicted in Fig. 2(a). The HST height H, chosen as the characteristic length, is 3.8 m. The dimensionless width and total length of the HST are 0.94H and 21.5 H, respectively. The head car and tail car are equipped with the trailer bogies while the middle car has the power bogies. The primary components of the trailer bogie and power bogie are presented in Fig. 2(b) and 2(c). The wheelbase of the both trailer and power bogies are D=2.5 m.

For the improvement of the snow-resistance ability of HSTs, the combined flow control scheme has been designed to keep the fixed inclined angles of the front plates of 60° and rear plates of 45°, as shown in Fig. 3(b). The proposed flow control scheme is made up of the front anti-snow structures and the rotational rear plates with deflecting angle of 45°. The former consists of the front air cylinder, front sliding plate, front deflecting plate and the rotational front plate, and the later is made up of the rear air cylinder, rear sliding plate, rear deflecting plate and the rotational rear plate, as depicted in Fig. 3(c). Taking the example with the operating direction in left direction, the workflow of the combined flow control scheme are described as follows.

Step 1: The front air cylinder pushes the rotational front plate and rotate the front plate counterclockwise to increase the inclined angles to 60°.

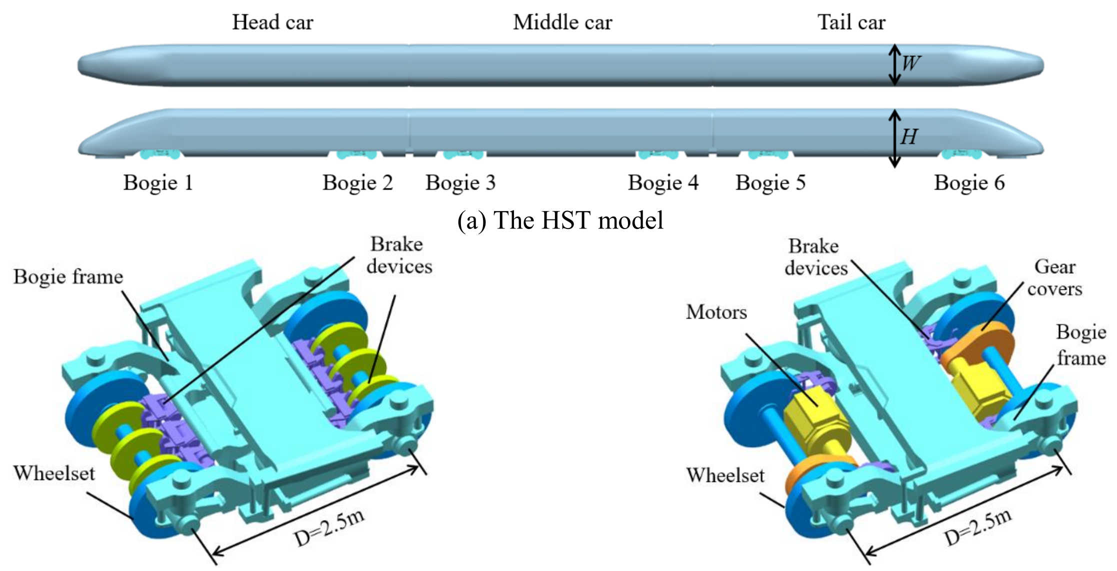

(a) The HST model

(b) Trailer bogie (c) Power bogie

Fig. 2 The selected HST models in the simulations

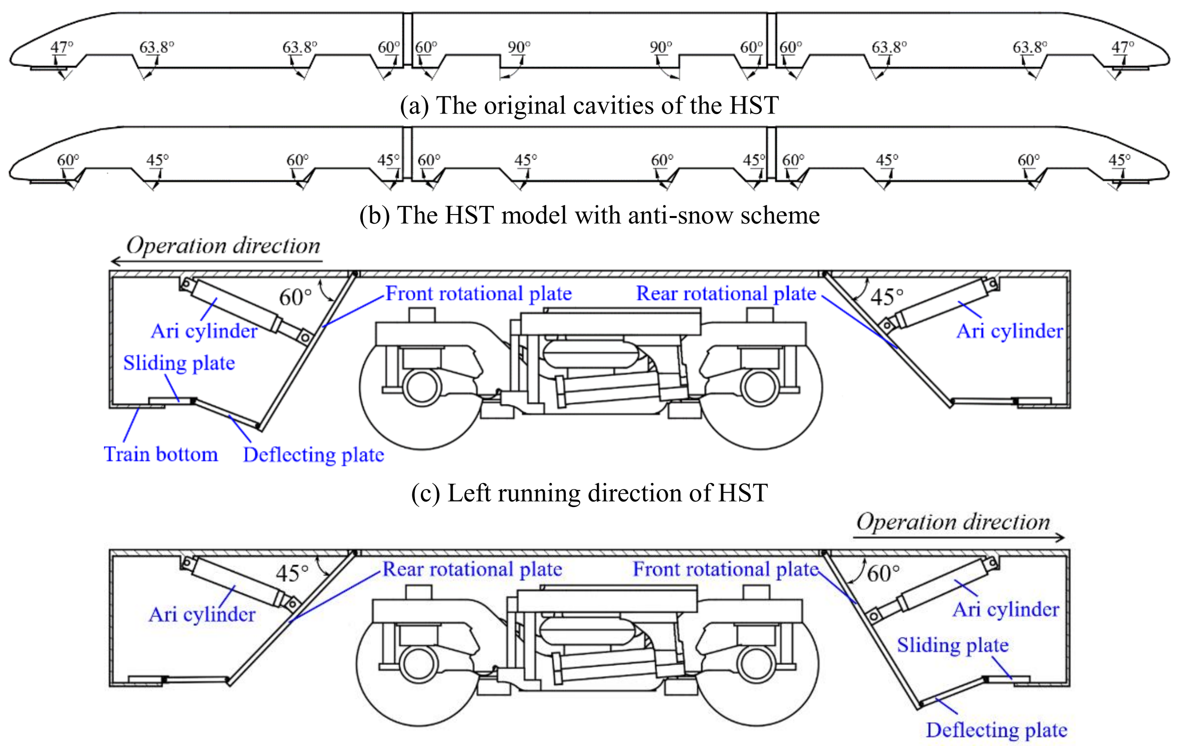

(a) The original cavities of the HST

(b) The HST model with anti-snow scheme

(c) Left running direction of HST

(d) Right operating direction of HST

Fig. 3 Sketch of the combined flow control scheme and the working status of the combined flow control scheme

Step 2: The rotational front plate forces the front deflecting plate to rotate clockwise by 30° around the connecting vertex of the front sliding plate.

Step 3: The front sliding plate moves downstream along the train bottom surface in the horizontal direction.

Step 4: The rear air cylinder pulls the rotational rear plate and rotates it counterclockwise to decrease the inclined angle to 45°.

Step 5: The rear deflecting plate pushes the rear sliding plate to move downstream along train bottom surface and finally keeps itself parallel to the horizontal direction.

Because of the HSTs usually run back and forth on the railways, the proposed flow control scheme needs to be installed at both upstream and downstream sides of the cavities. When HSTs run in the right direction, the work status of the flow control scheme is presented in Fig. 3(b), which can keep the same configuration of the cavities as for the left running direction.

2.2 Computational domain and boundary conditions

Fig. 4(a) shows that the HST model is arranged in a

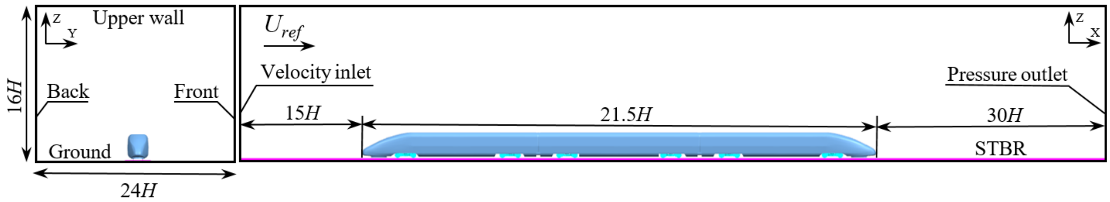

(a) Computational domain

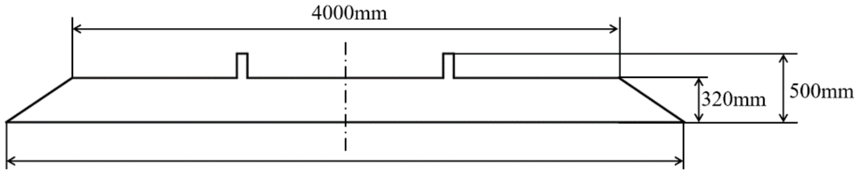

(b) Dimensions of the subgrade

Fig. 4 Computational domain

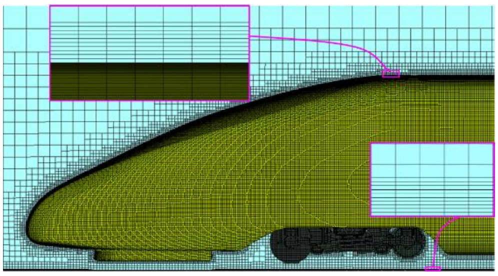

(a) Prism layer meshes distribution

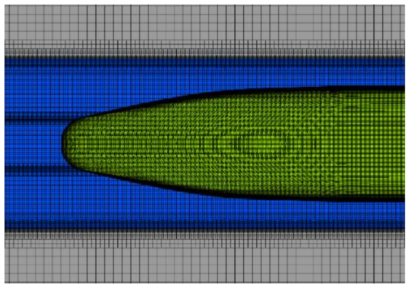

(b) Mesh distribution on the subgrade

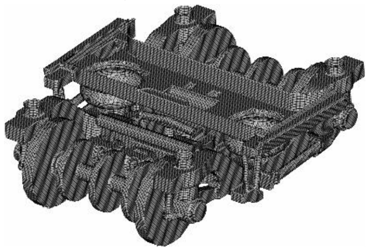

(c) Mesh distribution on the trailer bogie

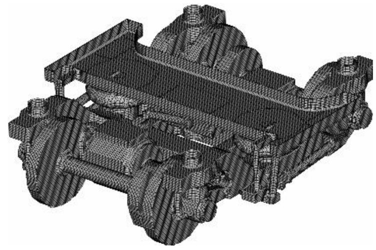

(d) Mesh distribution on the power bogie

Fig. 5 Computational mesh (medium resolution) distribution on the HST model

hexahedral computational domain with the dimensions of 66.5 H×24 H×16 H in the streamwise, spanwise and vertical directions, respectively. Additionally, the HST is mounted on the subgrade to reproduce a realistic operational environment (CEN European Standard 2013), and the detailed dimensions is presented in Fig. 4(b).

The outlet is given a zero static pressure. The front, back and upper surfaces of the domain were considered as symmetry condition. The subgrade and ground were set as moving walls with the same speed as that applied at the inlet. The outlet is given a zero static pressure. For the important impact of incoming airflow features on the underbody flow, in present study, the characteristics of the incoming flow was simulated by the turbulent kinetics energy, k, and the turbulent dissipation rate, ε. Both of these parameter k and ε were calculated by Eq. (1) and (2), respectively.

$$k = \frac{3}{2}(IU_{ref})^2 \tag{1}$$

$$\varepsilon = \rho C_\mu \frac{k^2}{\mu}\left(\frac{\mu_t}{\mu}\right)^{-1} \tag{2}$$

Here, the average speed of the incoming wind applied at the inlet, U_{ref}, was set as 55.56 m/s. I, the turbulent intensity, was considered to be 1%; the turbulent viscosity ratio, μ_t/μ, was considered to be 1.0; C_μ, was selected as 0.09; μ and ρ are the dynamic air viscosity and density at -30°C, μ=1.57e^{-5} Pa•s and ρ=1.453kg/m^3, respectively.

2.3 Grid generation

The openFOAM 5.0 was adopted to obtain the hexahedral-dominated computational grids around the HST, which ensures the maximum skewness of every cells was below 4.0. Skewness is defined as the distance from the face centre to the intersection of the line between the two adjacent cell centres which is then normalised by the centroid-to-centroid distance of the adjacent cell. This grid

Table1 Spatial resolution for Corse, medium and fine grids

Grids	n (mm)	Δs (mm)	Δl (mm)	$y^+=nU^*/v$	$z^+=\Delta sU^*/v$	$x^+=\Delta lU^*/v$	Cell numbers
Coarse	0.217	3.255	3.255	40	600	600	17 million
Medium	0.217	2.306	2.306	40	425	425	34 million
Fine	0.217	1.628	1.628	40	300	300	68 million

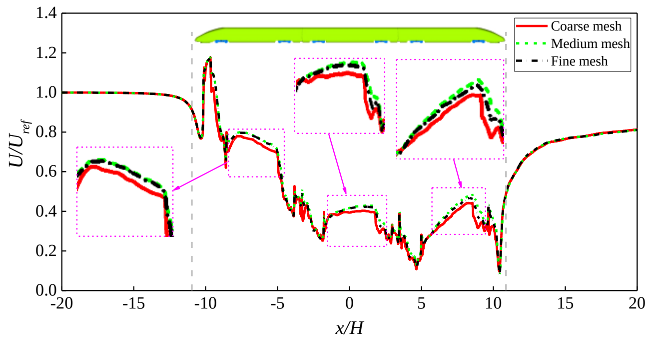

Fig. 6 Mean U distribution beneath the HST predicted by various grids

method has been wildly employed for the mesh generation in HST aerodynamic predictions (Niu *et al*. 2017, Niu *et al*. 2018, Zhang *et al*. 2018, Li *et al*. 2019, Xie *et al*. 2018, Guo *et al*. 2018, Gao *et al*. 2018b, Gao *et al*. 2019, Chen *et al*. 2019, Wang *et al*. 2019a). Ten prism layers applied to the HST were used to accurately capture the flow characteristics in the boundary layer, as presented in Fig. 5(a). Furthermore, Fig. 5(c) and 5(d) show the grids on the trailer and power bogies.

The mesh density study was also carried out using the Coarse, Medium and Fine grids, with the cell numbers of 17, 34 and 68 million, respectively. The sizes and spatial resolutions of the train surface cells in the coarse, medium and fine meshes are listed in Table 1. Here, U^* is the friction velocity, v is the kinetic viscosity, n is the distance between the first node and model surface along wall normal direction, Δl and Δs are the cell size in the streamwise and spanwise direction.

Fig. 6 compares the mean velocity magnitude U distribution along a streamwise sampling line predicted by the Coarse, Medium and Fine meshes. This streamwise sampling line, embedded in the centre plane (y/H=0), is 0.032H from the subgrade top. The comparison in Fig. 6 shows that the U value predicted by Coarse grid presents obvious error with the Fine case, especially near the cavities. This indicates an inadequate grid resolution of Coarse case, while the mean U profile in Medium case shows good agreement with that in Fine case. Thus, the Medium grid with 34 million cells was adopted to predict the flow fields around the cavities of the HST.

2.4 Numerical method

In this paper, URANS based on the Realizable k-ε turbulence model is employed to predict the airflow around the HST. To simulate the snow motion beneath the HST, the DPM is used. The detailed description of the numerical method URANS coupled with DPM, the numerical settings, and related parameter selections have been provided in previous study (Wang *et al.* 2019b). The numerical simulations were carried out using ANSYS Fluent 16.0 based on the Finite Volume Method and a pressure-based solver. The second-order upwind scheme was adopted for discretizing the convective fluxes in the k and ε formulas. Two way coupling algorithm between snow and airflow was adopted. The time-independent calculations of snow and airflow were conducted using a physical time-step size of 10^{-4}s. At every time step, the maximum value of iterations was 50, and the convergence criterions of the residuals of continuity, momentum, turbulence and DPM equations were set as 10^{-6}. The CFL number was less than 1.0 in more than 99% cells, with the maximum CFL of 3.0. All cases were initially calculated for t=2.0 s to obtain a converged field. After that, data sampling for time-dependent statistics is used to average the flow field, then the snow particles were injected into the domain, and the total simulation time is 6.0 s in every case.

It has been reported that the trajectories of snow particles are greatly affected by the following and inertial properties of the snow particles. For $S_{tk} \geq 1$, the snow particles will detach from the flow especially where the flow decelerates abruptly, and the movement characteristics are dominated by the particles' inertia property. For $S_{tk} \leq 1$, the snow closely follows the streamlines and the particles' trajectories are dominated by the following property.

$$S_{tk} = \frac{\rho_p d_p^2 U}{18\mu H} \tag{3}$$

where U is the local air velocity; d_p is the particle' diameter. In present study, small particles with d_p =0.15 mm is adopted. Based on the selection of particle size, the corresponding density ρ_p=916 kg/m^3 is chosen in all calculations.

At every time step, 3600 snow parcels were injected into the domain with the same speed as the incoming airflow. The snow particles were simplified as spheres and assumed to be unchanged before impacting on the bogies. For DPM boundary condition settings, the bogie frame, motors, brake calipers, gear covers, wheels and equipment cabin cover were set as trap conditions. In the trap condition, particles are considered to adhere to the bogies without rebounding splash as the snow impacts on the bogies. To ensure more snow flow into the cavities and cause more accretion, the HST, inter-carriage-gap and subgrade were set as reflect condition, and the snow particles will rebound off these surfaces with a change in its momentum as defined by the coefficient of restitution. The domain surfaces were set as escape condition, meaning the calculation of particle trajectory will be terminated as the particles encounter these surfaces.

3. Results and discussion

3.1 Algorithm validation

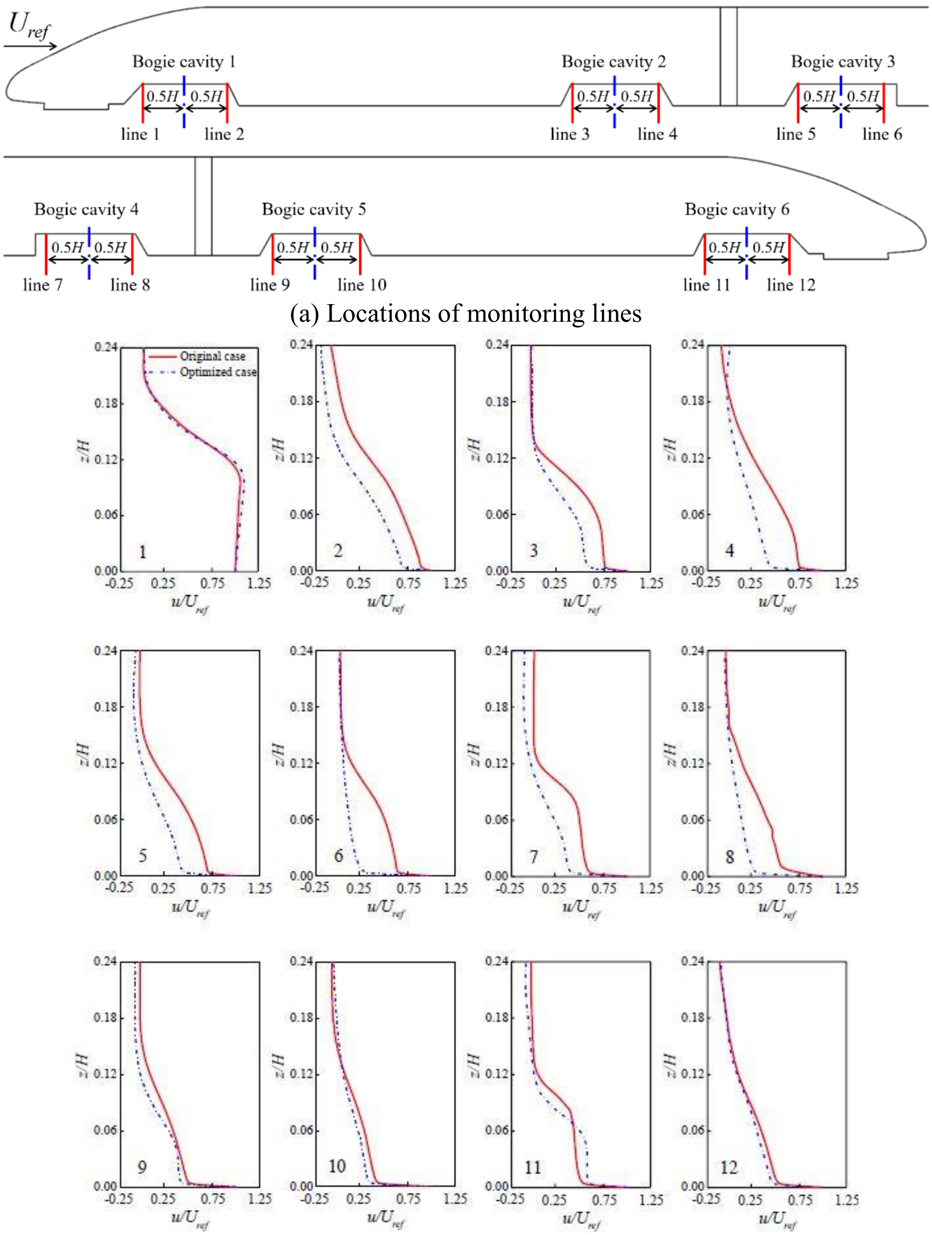

(a) Locations of monitoring lines

(b) *u* profiles

Fig. 7 Mean u distribution on various vertical monitoring lines predicted in two cases

The coupled numerical method of URANS and DPM for the investigation of the snow issue of the HST has been validated by the previous wind tunnel experiments (Xie *et al.* 2017, Wang *et al.* 2018a, Wang *et al.* 2018b, Gao *et al.* 2018a). To validate the simulation accuracy of the flow features in the bogie cavities, wind tunnel tests were conducted in the National Engineering Laboratory for High Speed Railway Construction of China, and the good agreement of flow trend and velocity distribution between the numerical and experimental results were obtained (Wang *et al.* 2018a, Wang *et al.* 2018b, Xie *et al.* 2017, Gao *et al.* 2018a). Furthermore, for the validation of the movement characteristics of the snow particles in the bogie cavities, the wind-snow tests for the HST were carried out in the High-speed Research Center of Central South University. A similar snow distribution on the bogies was observed from the comparison between the numerical results and the experimental results (Wang *et al.* 2018a, Wang *et al.* 2018b). This study used the same numerical method and optimal parameter settings (time-step size and total simulation time), thus, it's reasonable to assume current numerical method of URANS and DPM can be applied to study the snow issue of HST in present study.

3.2 Impact of the flow control scheme on the underbody flow characteristics

For the assessment of the influence of flow control scheme on train's snow-resistance ability, the comparison of velocity profiles of the airflow and snow particles, concentration level and accretion distribution in the bogie cavities at train's running speed of 200km/h will be carried

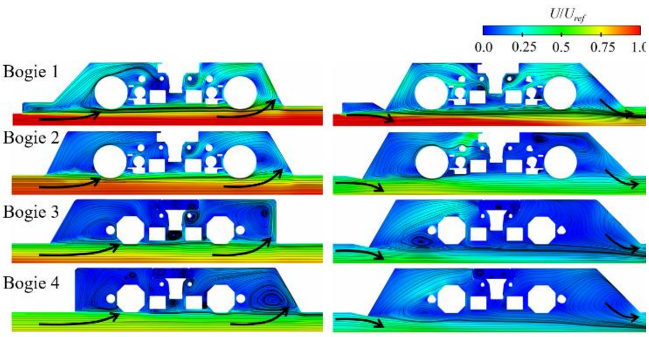

Fig. 8 Mean air streamlines on symmetric plane (y/H=0) in the cavities calculated in two cases

out in the following sections of 3.2, 3.3 and 3.4. Fig. 7 compares the mean streamwise velocity (u) distribution on the vertical monitoring lines in the cavities and the locations of these sampling lines are given in Fig. 7(a). Figure 7(b) shows that optimized case equipped with the combined flow control structure presents lower u value than the original case, especially from the subgrade (z/H=0) to the bottom surface of HST (z/H=0.12). This suggests that front anti-snow structures installed upstream the cavities can significantly deflect the airflow downwards at the entrance of the cavities and thereby decrease the u value in the underbody flow. Compared with the original case, the optimized case also presents lower u value in the vicinity of the rear parts of the cavities. This indicates that the optimized case can obviously weaken the strong impact on the rear plates caused by high-speed airflow.

Fig. 8 compares the mean velocity magnitude (U) distribution on symmetric plane (y/H=0) around the bogie cavities and in-surface projected time-averaged velocity streamlines. Fig. 7 suggests that the flow control scheme primarily affects the velocity distribution beneath the head and middle cars, thus, the comparisons of velocity distribution and streamlines are conducted in the cavities of head and middle cars. Fig. 8 shows high-speed airflow primarily move beneath the bogies while low-speed streamlines mainly move in the upper cavities. Previous study has proven that the snow tends to move with the high-speed airflow (Wang *et al.* 2018a). Thus, the high-speed streamlines will drive a great number of snow particles to directly impact on the bogies, leading to serious snow accretion on the bogie bottom. Besides, streamlines accompanied with relative low speed, flow upwards at the middle parts of the cavities and the rear plates, leading to several low-speed vortices. The low-speed streamlines will carry few snow to flow into the upper cavities and cause less snow on the top. The high-speed airflow at cavity entrance flow downwards due to the deflecting effect of the front anti-snow structures, which will weaken the strong impact on the windward surface of the bogies. This also indicates that the front anti-snow structures can lower the vertical flow range of snow particles and decrease the particles' concentration level near the key components of the bogies. Additionally, the rotational rear plates with the inclined angle of 45° in the optimized case are found to deflect downward the airflow and prevent the streamlines

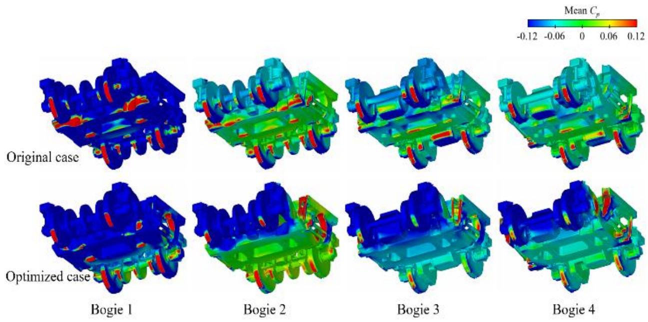

(a) C_p distribution on the bogies

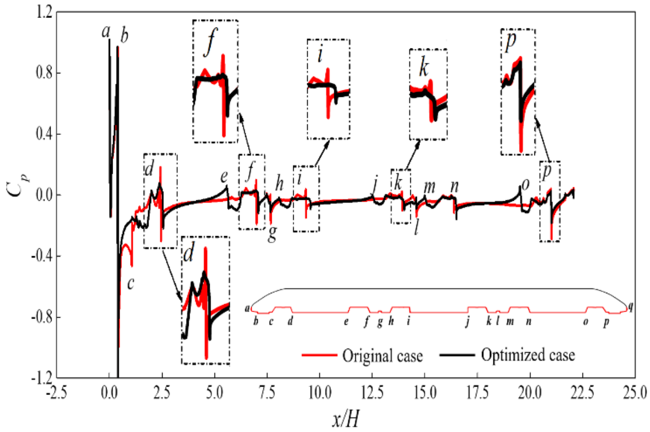

(b) C_p on the bottom centreline of HST

Fig. 9 Mean pressure coefficient (C_p) distribution on HST underbody structures

climbing upward along the rear plates, and thus decrease the particles' concentration level in the vicinity of the rear plates and upper cavities.

Fig. 9 presents the pressure coefficient (C_p) distribution on the underbody structures of the HST. It can be seen from Fig. 9(a) that the original case shows obvious positive C_p distribution on the primary heat-producing components (motors, brake devices and gear covers) caused by the high-speed underbody airflow. The airflow accompanied with massive snow directly impacts and adheres on the surfaces of these heat-producing components. However, these positive C_p distribution almost disappear in the optimized case, which will decrease the snow packing on the bogie bottom. Fig. 9(b) shows the mean C_p on train's bottom centreline. The positive values of C_p at the rear plates decrease obviously in the optimized case when compared the original case. This indicates that the proposed front anti-snow structures can significantly alleviate strong impact on rear plates caused by the airflow and the snow particles.

3.3 Effects of flow control scheme on the movement and distribution of snow particles

Fig. 10 compares the mean streamwise velocity of the snow particles (u_p) along the vertical sampling lines, and the locations of these sampling lines are provided in Fig. 7(b). Fig. 10 shows that the particle's streamwise velocity in the optimized case is obviously lower, when compared to original case. This suggests that the particle's kinetic energy

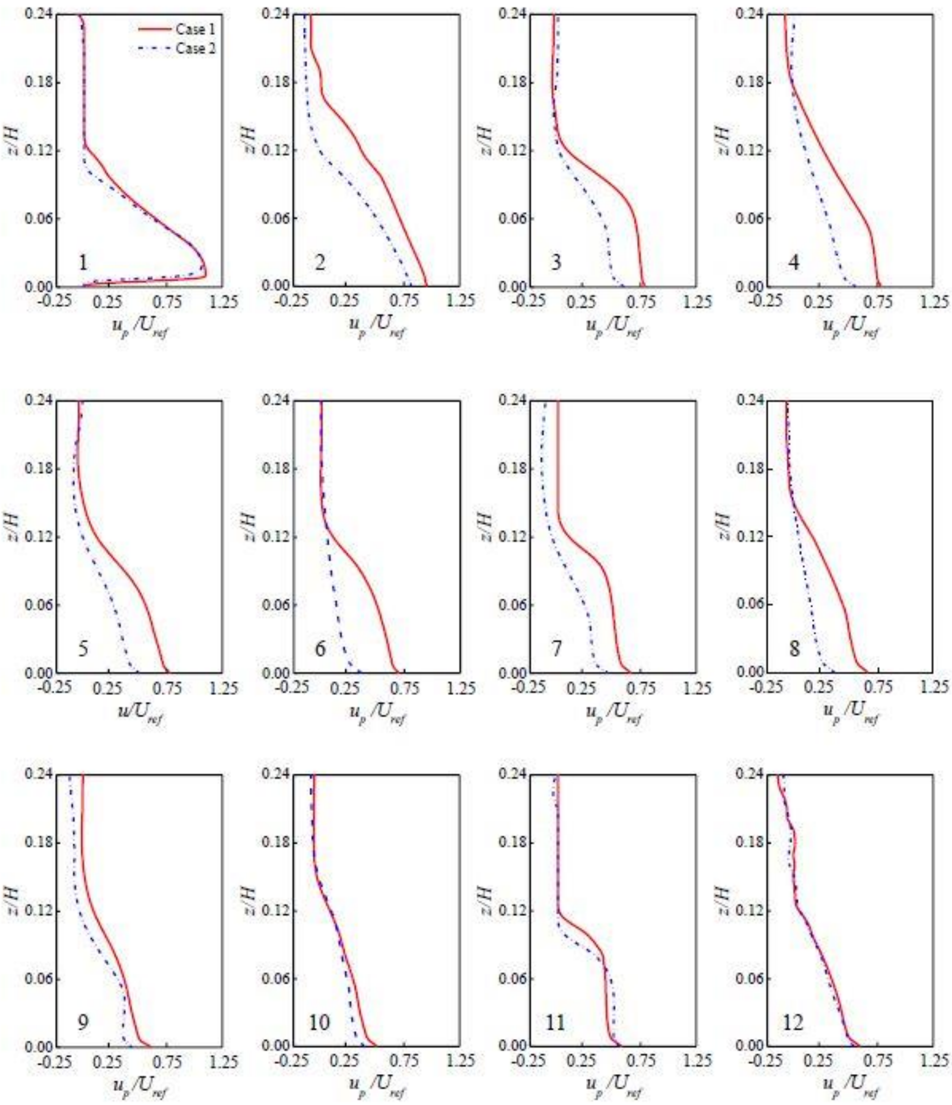

Fig. 10 Mean u_p profiles around the cavities of the HST

driving the snow particles to impact on the bogie surfaces and rear plates decreases obviously by installing the flow control scheme beneath the HST. Besides, the anti-snow scheme shows larger influence on altering the u_p profiles in the cavities of the head and middle cars, thus, we select cavity 2 and cavity 3 to perform the comparison of particle's velocity distribution and concentration level, for the assessment of the effects of flow control scheme on the particles' motion and concentration in the bogie cavities.

Fig. 11 presents the u_p distribution around the cavity 2 and cavity 3 calculated in two cases. It shows that the u_p value decreases obviously in the optimized case, showing good agreement with the finding in Fig. 10. Compared to the original case, the u_p distribution near the primary heat-producing components is much lower in the optimized case. This indicates that the front anti-snow structures in the optimized case can optimized the snow trajectory at the cavity entrance and thereby weaken the strong impact caused by the massive snow, which is relevant to the snow reduction for bogies.

Fig. 12 compares the particle's mean vertical velocity distribution w_p around the cavity 2 and cavity 3 between two cases. In the original case, the snow particles flow horizontally at the entrance of the cavities while they are deflected downwards in the optimized case. This suggests that the anti-snow structures can effectively optimize the particles' trajectories at the entrance to alleviate particles' impact on the bogies. Furthermore, the original case shows obvious positive w_p distribution at the rear plates while the optimized case presents the negative value. Additionally, Fig. 11 shows that the negative u_p distribution near the rear plates is clearly observed in the original case, and this negative u_p distribution shows less obvious in the optimized case. Combined the distribution characteristics of u_p and w_p near the rear plates, it can be concluded that the snow particles flow upwards at the rear plates and then move back to the upper cavities in the original case, leading to accumulated snow on bogie top. However, this phenomenon almost disappears in the optimized case, which is beneficial for the snow reduction of the top surface of the bogies.

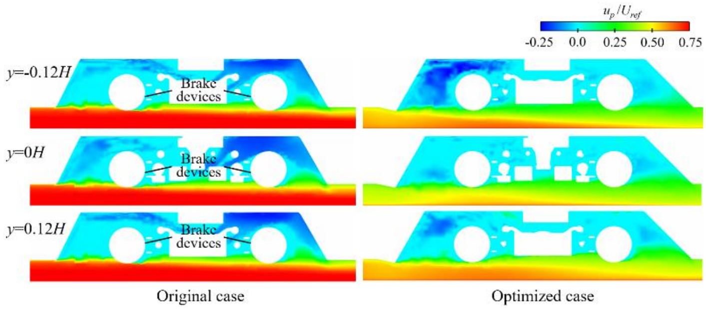

(a) Cavity 2

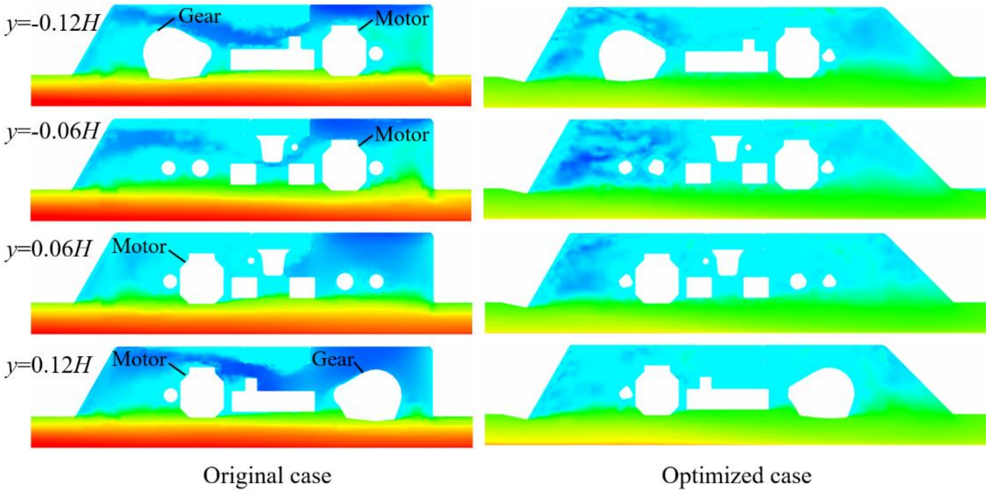

(b) Cavity 3

Fig. 11 Mean u_p distribution around cavity 2 and cavity 3 in two cases

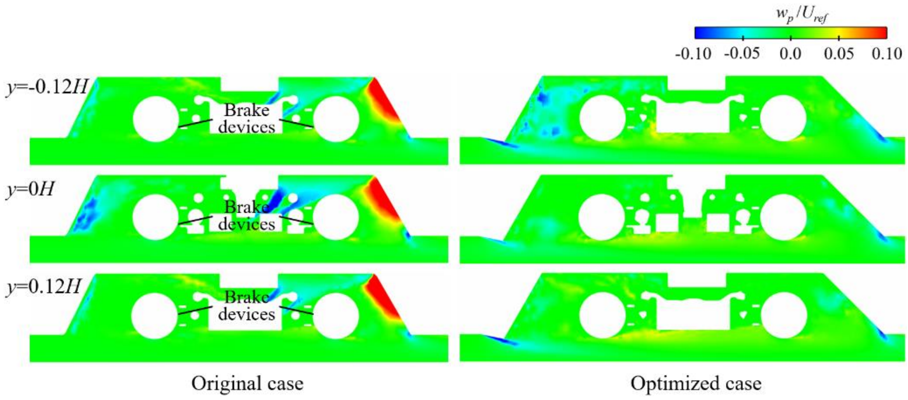

(a) Cavity 2

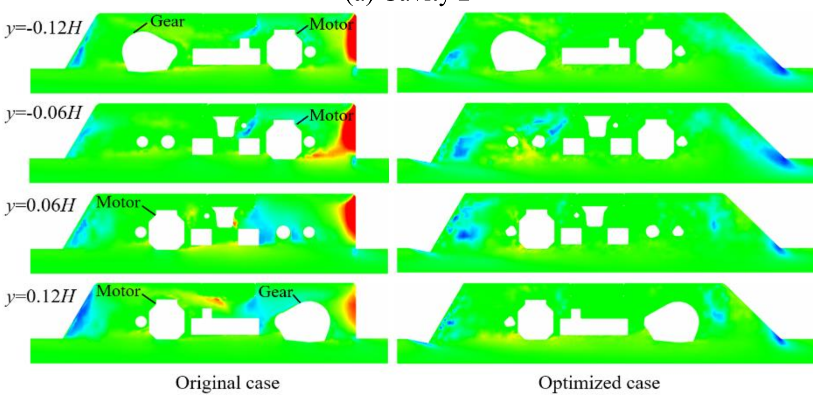

(b) Cavity 3

Fig. 12 Mean w_p distribution around bogie 2 and 3 cavities in two cases

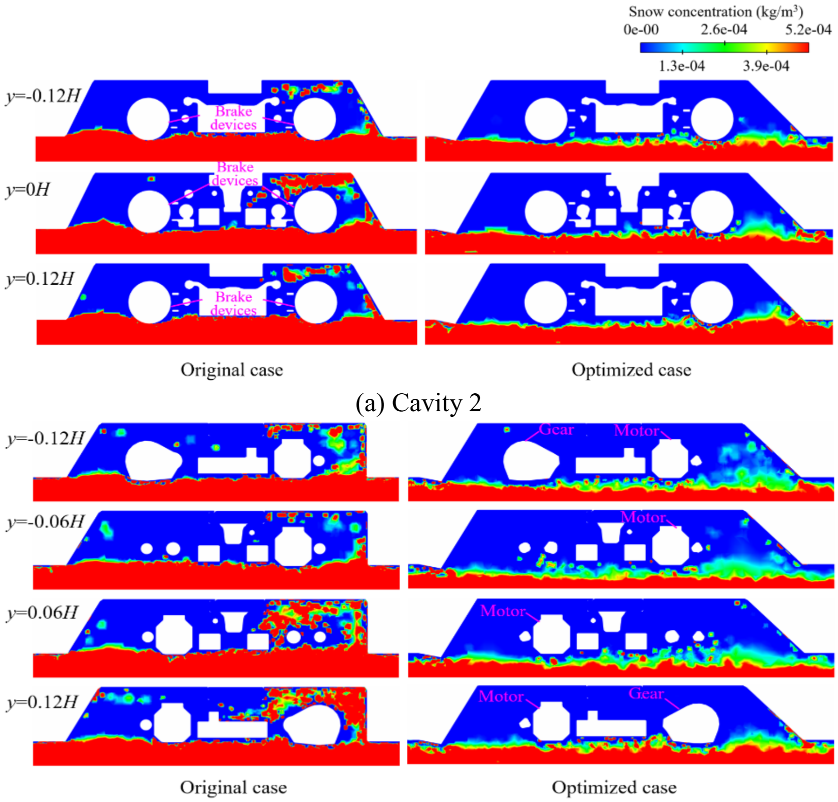

Fig. 13 Comparison of the snow concentration level around the cavities in two cases at t=6.0 s

Fig. 13 compares the snow concentration level in the bogie cavities between two cases at the simulation time of t=6.0 s. The flow range of snow particles with high concentration value in the vertical direction becomes much lower in the optimized case, especially at the primary heat-producing components. This is because the front anti-snow structures force the airflow and snow to flow close to the subgrade. Previous studies have proven that the particles' upward climbing along the rear plate causes snow accretion on the rear plates and the upper surface of the bogies (Wang *et al.* 2018a, Wang *et al.* 2019b). The rotational rear plates with the deflecting angle of 45° in the optimized case significantly reduce the particle's amounts moving near the rear plates and suspending above the bogies, thereby decreasing the accretion on bogie top. Therefore, combined flow control scheme can optimized the particles' trajectories at both the entrance and outlet of the cavities, by deflecting downwards the snow particles at the entrance and forcing more particles to flow out of the cavities at the outlet.

3.4 Influence of flow control scheme on the snow accretion in the cavities

Fig. 14 compares the snow accretion on bogie 2 and bogie 3 at t=6.0 s between two cases. Generally, the snow accretion on the bogie bottom is much more than that on the top. This is because most of the snow particles driven by the high-speed airflows at the lower cavities directly impact and adhere on the bogie bottom, while less snow possess enough energy to overcome the gravity and flow into the upper cavities. Compared with the original case, the accretion on the bottom decreases obviously in the optimized case, especially at the primary heat-producing equipment, owing to the downward deflecting effect on the particles' trajectories at the entrance of the cavities. For the comparison of the snow accretion on the top of the bogies, the optimized case shows very less snow than the original case. The explanation for this is twofold. As shown in Figs. 11 and 12, the positive streamwise and vertical speed decrease obviously in the optimized case, indicating that the front anti-snow structures can effectively lower the kinetic energy to support the snow particles to flow into the upper parts of the cavities. Another reason is that the rotational rear plates with the deflecting angle of 45° presents well guiding effect at the outlet of the cavities, and thus forces more snow to flow out of the cavities.

Previous studies (Wang *et al.* 2018a) have found that the snow mass on the primary components of the bogies during per 0.5s is basically the same when the calculating time reaches 2.0s. Therefore, the snow mass on the bogies during the last 0.5s can be used to evaluate the effect of the combined flow control scheme on the snow reduction. Figure 15 lists the snow mass of key components of bogie 2 (trailer bogie) and bogie 3 (power bogie) in two cases within the time period from t=5.5 s to t=6.0 s. Compared to the original case, the accretion mass of brake devices, bogie frame and rear plate around cavity 2 in the optimized case decreases by around 24%, 38% and 28%. Furthermore, the accumulated mass on the brake devices, bogie frame, rear plate, motors and gear covers around cavity 3 reduces by approximately 22%, 33%, 30%, 45% and 36%, respectively. These results presented above indicate that the combined

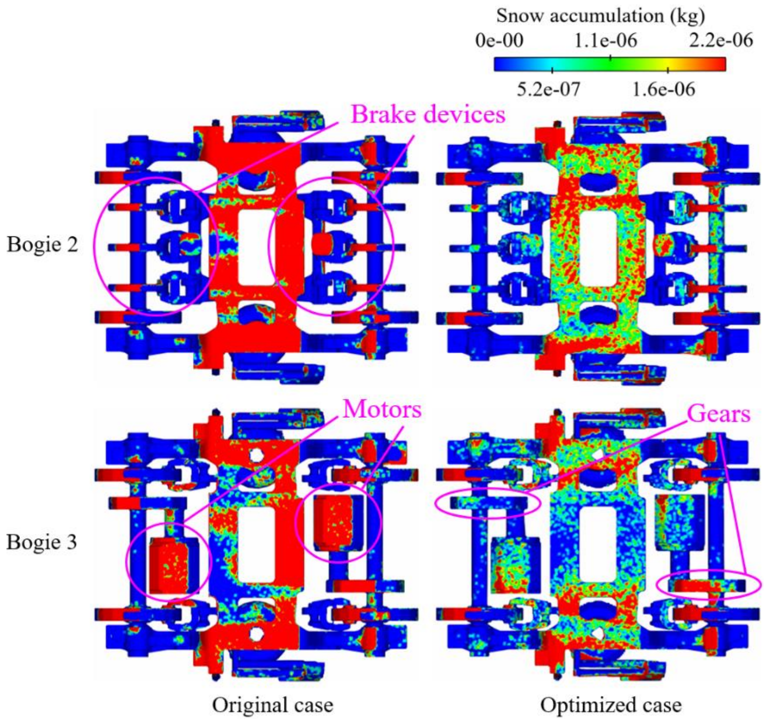

(a) Bottom surface of the bogies

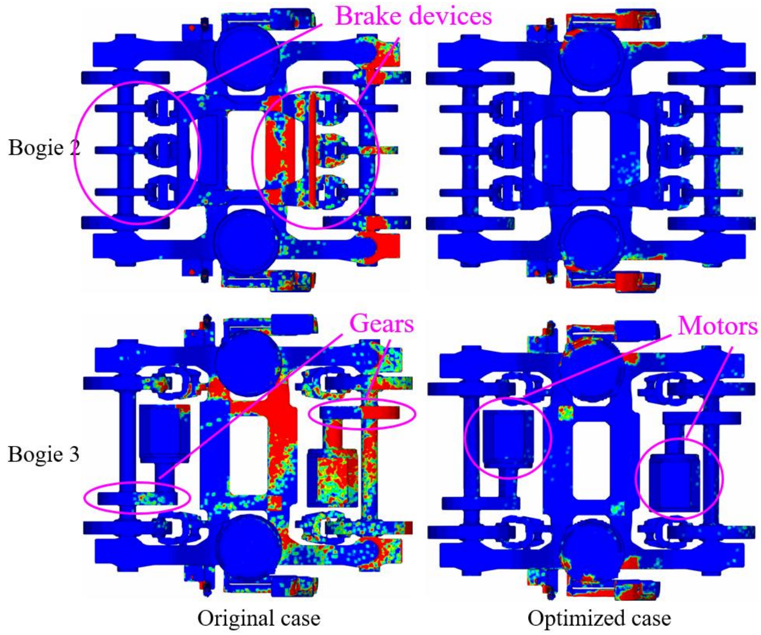

(b) Top surface of the bogies

Fig. 14 Accumulated snow on the bogie 2 and bogie 3 at t=6.0 s

flow control is beneficial for the snow reduction of HST.

3.5 Capability of the anti-snow scheme at higher running speed of HST

The numerical results discussed before suggests that the proposed combined flow control scheme is obviously effective to decrease the accretion mass on the bogies at the running speed of 200 km/h. While the operating speed of the HSTs in the snowy and cold regions in China varies from 200 km/h to 300 km/h. The running speed of HST has been found to significantly affect the accretion mass in the cavities (Wang *et al.* 2018c), and the proposed anti-snow scheme will certainly result in various deflecting effect at different running speed. Thus, the purpose of this section is to verify whether this combined flow control scheme also benefits the snow reduction for the HSTs running at higher running speed.

Fig. 16 compares the accumulated mass of the bogies from the calculating time 5.5 s to 6.0 s at various HST operating speed between the original case and optimized case. The general observation in Fig. 16 is that the accretion

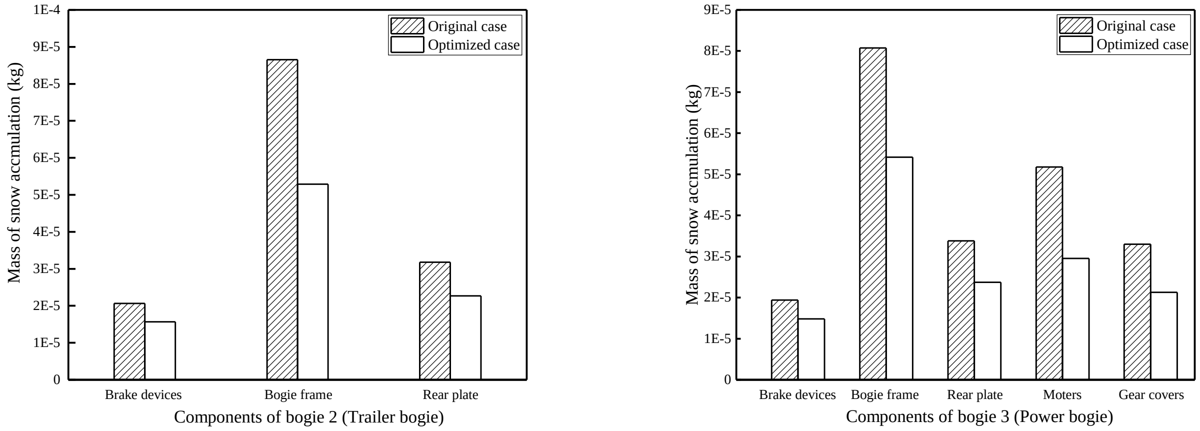

Fig. 15 Accumulated mass on the components of bogie 2 and bogie 3 from t=5.5 s to 6.0 s

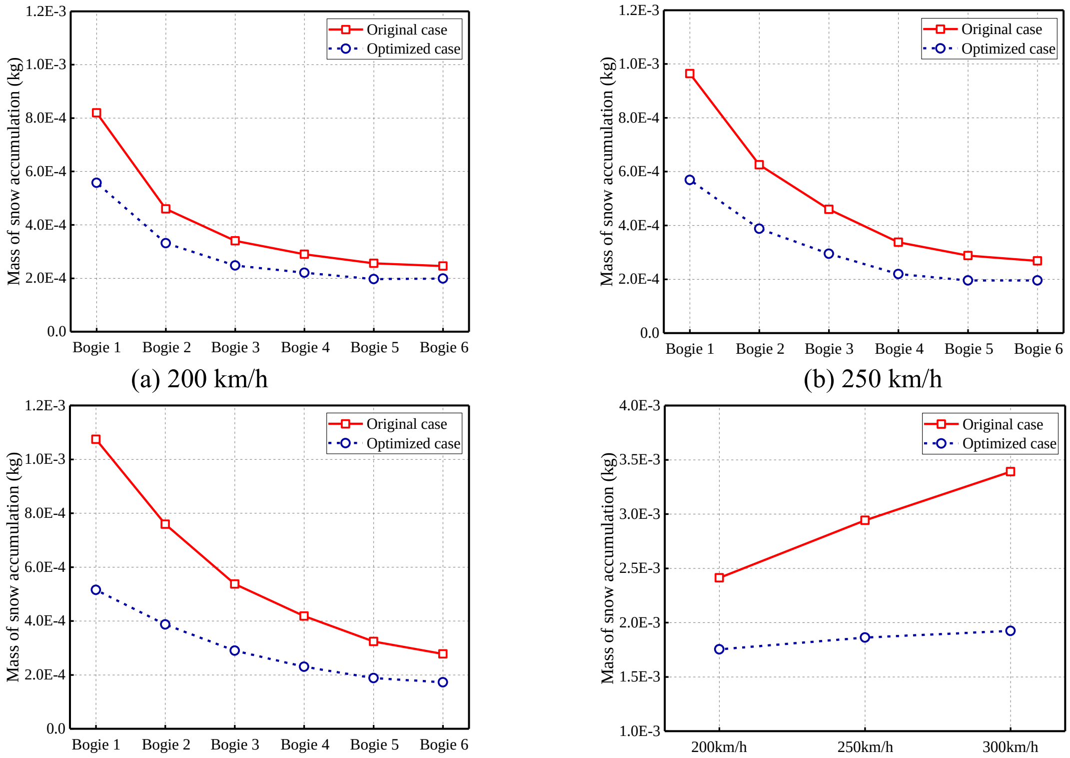

(a) 200 km/h (b) 250 km/h

(c) 300 km/h (d) Comparison for two cases

Fig. 16 Comparison of the snow mass packing on the bogies within the simulation time from 5.5s to 6.0s at different HST running speeds between the original case and optimized case

mass of bogies reduces along the streamwise direction in all cases, in which the bogie 1 presents the most snow while the last has the least. Furthermore, in Fig. 16, an obvious snow reduction is found in the optimized case, compared with the original case. When the HST runs at the speed of 200 km/h, the snow accumulation of bogie 1 to bogie 6 in the optimized case reduces by approximately 32%, 28%, 27%, 24%, 23% and 19% respectively, compared to the original case. As the running speed reaches 250 km/h, the rates of snow reduction in the optimized case for the bogie 1 to bogie 6 are around 41%, 38%, 36%, 35%, 32% and 27%. These corresponding numbers at the operating speed of 300 km/h are about 52%, 49%, 46%, 45%, 42% and 38%, respectively. Moreover, the total mass of snow accumulation on all bogies is found to decrease by 27.27% (200 km/h), 36.72% (250 km/h) and 47.41% (300 km/h) in the optimized case, indicating that the proposed flow control scheme presents better anti-snow performance and achieve more snow reduction when HST runs at higher speed.

4. Conclusions

This paper numerically investigates the improvement of the snow-resistance ability for a three-car grouped HST based on the passive flow control method. The accuracy of the coupled numerical methods of URANS and DPM have been validated against previous wind tunnel tests.

The optimization of the anti-snow performance is twofold. On the one hand, the front anti-snow structures installed upstream the cavities have dominant influences on the flow characteristics and the particles' trajectories in the bogie cavities, by deflecting downwards the airflow and snow particles at the entrance of the cavities. This effectively alleviates the strong impact on the bogie bottom and lower particles' concentration value near the main heat-producing components, thereby decrease accretion mass on the bogie bottom. Secondly, the proposed flow control structures are found to significantly decrease the accretion distribution on bogie top. This is because the front anti-snow structures can reduce the streamwise velocity distribution of both airflow and snow around the cavities, and decrease the particles' kinetic energy supporting the snow to flow into the upper cavities. Another reason for this is that the rotational rear plates with the deflecting angle of 45° play an important role in guiding the airflow and snow near the cavity outlet, and reducing the amount of snow particles suspending above the bogies.

Besides, the capability of the anti-snow structures has been also studied at the various running speeds of HST (200km/h, 250km/h and 300km/h). The proposed combined flow control scheme is found to present better anti-snow performance in the case with higher HST speed. Compared to the original case with the HST speed of 250 km/h, the accumulated mass of all bogies decreases by 27.27% in the optimized case. The corresponding snow reduction at the operating speed of 250 km/h and 300 km/h are 36.72% and 47.41%, respectively. Therefore, the proposed anti-snow structures have a positive influence on the improvement of the running safety of HSTs in the cold regions, especially at higher train's running speed.

Acknowledgements

The authors acknowledge the computing resources provided by the High-speed Train Research Center of Central South University, China.

This work was accomplished by the supports of the National Key Research and Development Program of China [Grant No. 2017YFB1201304], the Hunan Provincial Innovation Foundation for Postgraduates [Grant No. 150110003], the Free Exploration and Innovation Project for Postgraduates of Central South University [Grant No. 502221905].

References

Bettez, M. (2011), "Winter technologies for high speed rail", Master's Thesis, Norwegian University of Science and Technology, Norway.

Casa, X.D.L., Paradot, N. Allain, E. Pauline, J. Delpech, P. and Bouchet, J.P. (2014), "A numerical modelling of the snow accumulation on a high-speed train", *International Conference in Numerical and Experimental Aerodynamics of Road Vehicles and Trains*, Bordeaux, France, June.

CEN European Standard (2013), "Railway applications-aerodynamics. part 4: requirements and test procedures for aerodynamics on open track", Research Report No. CEN EN 14067-4.

Chen, G., Li, X.B. Liu, Z. Zhou, D. Wang, Zhe. Liang, X.F. and Krajnovic, S. (2019), "Dynamic analysis of the effect of nose length on train aerodynamic performance", *J. Wind Eng. Indus. Aerod*., **184**, 198-208. https://doi.org/10.1016/j.jweia.2018.11.021.

Ding, S.S., Tian, A.Q. Dong, T.Y. Zhou, W. and Li, J.J. (2016), "Influence of inclined guiding plate on anti-snow performance of high-speed train bogie", *J. Central South Univ*., **4**, 1400-1406.

Fluent Inc. (2011), Fluent User's Guide.

Fujii, T., Kawashima, K. Iikura, S. Endo, T. and Izunami, R. (2002), "Preventive measures against snow for high-speed train operation in Japan", *11th International Conference on Cold Regions Engineering*, Alaska, U.S.A., May.

Gao, G. J., Li, F. He, K. Wang, J.B. Zhang, J. and Miao, X.J. (2019), "Investigation of bogie positions on the aerodynamic drag and near wake structure of a high-speed train", *J. Wind Eng. Indus. Aerod*., **185**, 41-53. https://doi.org/10.1016/j.jweia.2018.10.012.

Gao, G.J., Zhang, Y. Xie, F. Zhang, J. He, K. Wang, J.B. and Zhang, Y.N. (2018a), "Numerical study on the anti-snow performance of deflectors in the bogie region of a high-speed train using the discrete phase model", *Proceedings of the Institution of Mechanical Engineers Part F Journal of Rail & Rapid Transit*, **233**(2), 141-159.

Gao, G.J., Zhang, Y.N. Zhang, J. Xie, F. Zhang, Y. and Wang, J.B. (2018b), "Effect of bogie fairings on the snow reduction of a high-speed train bogie under crosswinds using a discrete phase method", *Wind Struct*., **27**(4), 255-267. https://doi.org/10.12989/was.2018.27.4.255.

Giappino, S., Rocchi, D. and Schito, P. (2016), "Cross wind and rollover risk on lightweight railway vehicles", *J. Wind Eng. Indus. Aerod*., **153**, 106-112. https://doi.org/10.1016/j.jweia.2016.03.013.

Guo, Z.J., Liu, T.H. Chen, Z.W. Xie, T.Z. and Jiang, Z.H. (2018), "Comparative numerical analysis of the slipstream caused by single and double unit trains", *J. Wind Eng. Ind. Aerod*., **172**, 395-408. https://doi.org/10.1016/j.jweia.2017.11.022.

Kosinski, P. and Hoffmann, A.C. (2007), "An eulerian-lagrangian model for dense particle clouds", *Comput. Fluids*, **36**(4), 714-723. https://doi.org/10.1016/j.compfluid.2006.06.003.

Li, X.B., Chen, G. Wang, Z. Xiong, X.H. Liang, X.F. and Yin, J. (2019), "Dynamic analysis of the flow fields around single-and double-unit trains", *J. Wind Eng. Ind.. Aerod*., **188**, 136-150. https://doi.org/10.1016/j.jweia.2019.02.015.

Miao, X.J. and He, K. (2018), "Cause analysis of snow packing in high-speed train's bogie regions and anti-snow packing design", *J. Central South Univ*., **3**, 756-763.

Niu, J. Q., Wang, Y. M. Zhang, L. Yuan, Y. P. (2018), "Numerical analysis of aerodynamic characteristics of high-speed train with different train nose lengths", *Heat Mass Transfer*, **127**, 188-199. https://doi.org/10.1016/j.ijheatmasstransfer.2018.08.041.

Niu, J.Q., Zhou, D. and Liang, X.F. (2017), "Numerical simulation of the effects of obstacle deflectors on the aerodynamic performance of stationary high-speed trains at two yaw angles", *Proc. Inst. Mech. Eng. Part F. J. Rail Rapid Transp*, **232**(3): 913-927. https://doi.org/10.1177%2F0954409717701786.

Paulukuhn, L. and Wu, X. (2012), "The low temperatures technology concepts and operational experience in Russian high speed train velaro RUS", *Foreign Rolling Stock*, **49**(3), 16-19.

Wang, J., Minelli, G. Dong, T. Chen, G. and Krajnović, S. (2019a). "The effect of bogie fairings on the slipstream and wake flow of a high-speed train. An IDDES study", *J. Wind Eng. Ind. Aerod*., **191**, 183-202. https://doi.org/10.1016/j.jweia.2019.06.010.

Wang, J.B., Gao, G.J. Liu, M.Y. Xie, F. and Zhang, J. (2018a), "Numerical study of snow accumulation on the bogies of a high-speed train using URANS coupled with discrete phase model", *J. Wind Eng. Ind. Aerod*., **183**, 295-314. https://doi.org/10.1016/j.jweia.2018.11.003.

Wang, J.B., Gao, G.J. Zhang, Y. and Xie, F. (2017), "Numerical simulation of snow accumulation on a bogie of a high-speed train", *DEStech Transac. Eng. Technol. Res*. 771-778. 10.12783/dtetr/icia2017/15701.

Wang, J.B., Gao, G.J. Zhang, Y. He, K. and Zhang, J. (2019), "Anti-snow performance of snow shields designed for brake calipers of a high-speed train", *Proceedings of the Institution of Mechanical Engineers Part F Journal of Rail & Rapid Transit*, **233**(2), 121-140.

Wang, J.B., Zhang, J. Xie, F. Zhang, Y. and Gao, G.J. (2018c), "A study of snow accumulating on the bogie and the effects of deflectors on the de-icing performance in the bogie region of a high-speed train", *Cold Regions Sci. Technol*., **148**, 121-130. https://doi.org/10.1016/j.coldregions.2018.01.010.

Wang, J.B., Zhang, J. Zhang, Y. Liang, X.F. Krajnovic, S. and Gao, G.J. (2019b), "Impact of rotation of wheels and bogie cavity shapes on snow accumulating on the bogies of high-speed trains", *Cold Regions Sci. Technol*., **159**, 58-70. https://doi.org/10.1016/j.coldregions.2018.12.003.

Wang, J.B., Zhang, J. Zhang, Y. Xie, F. Krajnovic, S. and Gao, G.J. (2018d), "Impact of bogie cavity shapes and operational environment on snow accumulating on the bogies of high-speed trains", *J. Wind Eng. Indus. Aerod*., **176**, 211- 224. https://doi.org/10.1016/j.jweia.2018.03.027.

Xie, F., Zhang, J. Gao, G.J. He, K. Zhang, Y. Wang, J.B. and Zhang, Y. (2017), "Study of snow accumulation on a high-speed train's bogies based on the Discrete Phase Model", *J. Appl. Fluid Mech*. **10**, 1729-1745. http://10.29252/jafm.73.245.27410.

Xie, T.Z., Liu, T.H. Chen, Z.W. Chen, X.D. and Li, W.H. (2018), "Numerical study on the slipstream and trackside pressure induced by trains with different longitudinal section lines", *Proc. Inst. Mech. Eng. Part F. J. Rail Rapid Transp*, **232**(6): 1671-1685. https://doi.org/10.1177%2F0954409717744976.

Zhang, J., Wang, J.B. Wang, Q.X. Xiong, X.H. and Gao, G.J. (2018), "A study of the influence of bogie cut outs' angles on the aerodynamic performance of a high-speed train" *J. Wind Eng. Ind*., *Aerod*., **175**, 153-168. https://doi.org/10.1016/j.jweia.2018.01.041.

FR